Initial steps for the thermal decomposition of alkaline-earth metal amidoboranes: a cluster approximation†

A. V. Pomogaeva* and A. Y. Timoshkin

A DFT study of thermal decomposition mechanisms of $[M(NH_2BH_3)_2]_4$ clusters with M = Mg, Ca, and Sr is presented. Multi-step reaction pathways leading to elimination of the first H_2 molecule are explored at the M06/TZVP level of theory. For all studied M, the clusters adopt similar structures and exhibit similar transformations along the reaction pathways. Their activation energies decrease in the order Mg < Ca ≤ Sr. Four metal atoms in the cluster form a rigid planar construction that is found to be nearly unchanged during all transformations. Cleavage of the B–H bond in the environment of alkaline-earth metal atoms leads to the "capture" of the released H atom by neighboring metal atoms with the formation of a M_3H moiety. While the activation energies for the cleavage of $H^{\delta-}$ can be as low as 14.3, 22.6 and 23.3 kcal mol^{-1} for M = Mg, Ca and Sr, respectively, barriers for the subsequent cleavage of $H^{\delta+}$ *via* destruction of the M_3H moiety are about twice larger.

Introduction

Development of materials with properties appropriate for transportable hydrogen storage is an advanced field in modern chemistry.[1,2] The excellent gravimetric and volumetric hydrogen density of ammonia borane and its derivatives attracts persistent interest in this class of compounds.[3,4] It was found that alkali-metal amidoboranes $LiNH_2BH_3$ and $NaNH_2BH_3$ release more hydrogen at lower temperatures than pure ammonia borane and also suppress borazine release.[5] However, release of a significant amount of ammonia was observed under thermal decomposition of alkali-metal amidoboranes.[6–10]

Alkaline-earth amidoboranes $Mg(NH_2BH_3)_2$ (MgAB),[11] $Ca(NH_2BH_3)_2$ (CaAB),[12] and $Sr(NH_2BH_3)_2$ (SrAB)[13] are known laboratory species which also demonstrate improved dehydrogenation properties compared to ammonia borane. First, CaAB was obtained as a THF adduct,[14] then pure CaAB was synthesized by ball milling of CaH_2 and BH_3NH_3.[12] These forms have different dehydrogenation properties. THF containing CaAB releases H_2 mainly in the temperature range from 120 to 245 °C,[14] while the solvent free CaAB eliminates hydrogen at $\sim$80 °C with peaks at 100 and 140 °C.[12] H_2 release from SrAB starts at about 60 °C and the decomposition becomes violent as the temperature

increases to 93 °C. MgAB exhibits three overlapping dehydrogenation steps with the peak temperatures at 104, 162 and 223 °C.[11] Activation energies for the three dehydrogenation steps are 20.1, 27.7 and 28.4 kcal mol^{-1}. The third dehydrogenation step of MgAB is found to be mildly endothermic and the thermolysis of MgAB yields no volatile by-products.[11] Dehydrogenation of CaAB also is not accompanied by the release of borazine.[12] The release of B_2H_6 and NH_3 was noticed during the thermal decomposition of SrAB.[13]

Experimental success in the synthesis of alkaline-earth amidoboranes has stimulated related theoretical studies. A number of works based on solid state theory are devoted to the prediction of crystal structure,[15] dehydrogenation mechanisms,[16] possible intermediate products of the dehydrogenation reaction,[17] hydrogen diffusion pathways,[18] and optical[19] and elastic[20] properties of metal amidoboranes (MAB). Advantages of MAB over pure ammonia borane (lower dehydrogenation barriers, a less exothermic overall dehydrogenation reaction and borazine suppression) are attributed to the ionic character of bonds in MAB and the catalytic role of the metal. However, the detailed dehydrogenation mechanism is still unclear. Kim *et al.*[21] presented a comprehensive *ab initio* study of the mechanisms and kinetics of H_2 release in monomers and dimers of MAB. They concluded that oligomerization (O-path) and non-oligomerization (D-path) pathways are competitive. The oligomerization pathway is found to be more favorable for alkali-metal amidoboranes. In contrast, the release of H_2 *via* direct transfer of H^-, abstracted by the metal cation from the BH_3 group, to H^+ of the NH_2 group of the same NH_2BH_3 unit is more favorable in the case of CaAB and MgAB.

Inorganic Chemistry Group, Institute of Chemistry, St. Petersburg State University, Universitetskaya nab. 7/9, St. Petersburg, 199034, Russia.
E-mail: avpomogaeva@cc.spbu.ru

† Electronic supplementary information (ESI) available: Fig. S1–S6, Table S1, and optimized structures of all clusters. See DOI: 10.1039/c6cp05835c

The activation energy of the release of the first H_2 molecule from CaAB and MgAB is equal to 36 kcal mol^{-1} at the MP2/6-311++G** level of theory. Yuan et al.[22] reported that the release of the first H_2 molecule from the CaAB dimer is kinetically more favorable if it does not involve the Ca atom in the dehydrogenation transition state. No pathways of formation of an oligomeric $[BH_3NH_2BH_2NH_2]^-$ unit were found at the DFT(PBE/PAW) level of theory.[22]

These theoretical studies reveal the importance of intermolecular interactions for the particular development of chemical reactions in MAB. The crystal structure of these compounds features a network based on weak M–N and M–H(BH$_3$) interactions. Cluster approximation is an intermediate approach between molecular and solid state computations. It allows tracking of molecular transformations in the chemical reaction pathways taking into account the local atomic environment.[23,24] Herein, we present a comparative study of possible pathways leading to the release of the first molecule of H_2 from tetrameric clusters $[M(NH_2BH_3)_2]_4$, where M = Mg (**1**), Ca (**2**), and Sr (**3**).

Results and discussion

A. Structure of $[M(NH_2BH_3)_2]_4$ tetramers

In the present work, a tetrameric cluster, $[Ca(NH_2BH_3)_2]_4$ (**2**), was obtained by optimization of a cutout from crystalline CaAB. CaAB adopts a monoclinic structure with the C_2 space group.[12] Each Ca atom is coordinated with two NH_2 and four BH_3 groups (Fig. 1a). The minimal distance between H$^+$ and H$^-$ of adjacent layers is about 2.4 Å, i.e. no dihydrogen bonds occur. This observation points out that dehydrogenation proceeds within a layer. A chosen piece of crystalline structure is shown in Fig. 1a and the optimized geometry of the resultant C_{2h} symmetric tetrameric cluster is presented in Fig. 1b (projection onto the XY plane).
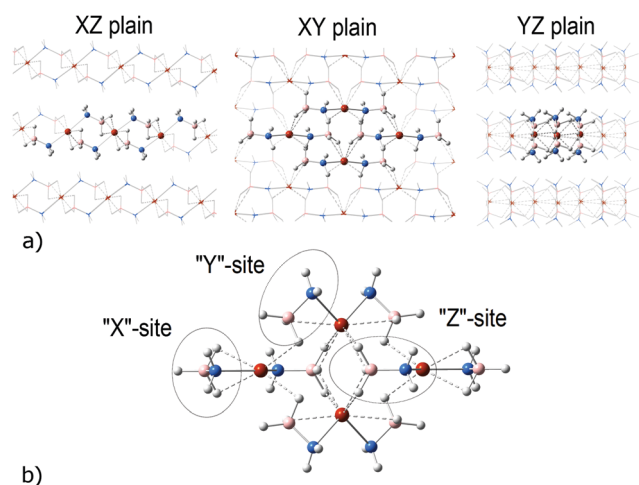

Fig. 1 Three projections of the experimental crystalline structure of CaAB[12] (a) and the optimized structure of $[Ca(NH_2BH_3)_2]_4$ (b). Molecules extracted from the crystal structure are shown in ball & bond format, other molecules are shown as a wireframe. Red refers to Ca atoms, blue to N, orange to B and white to H atoms. The Ca–H(BH$_3$) bond network is shown by dashed lines. "x"-, "y"- and "z" positions of NH$_2$BH$_3$ units are marked with ovals.

The z-axis is chosen to be perpendicular to the layer. NH_2BH_3 groups in the cluster can be classified according to their positions as shown in Fig. 1b. Expectedly, the Ca–N–B angles are the most affected by optimization, which is reflected in the formation of additional Ca–H(BH$_3$) bonds with x- and y-NH$_2$BH$_3$ groups. The environment of BH$_3$ groups in z-NH$_2$BH$_3$ is less affected upon the optimization of the cutout from the crystal tetramer. Overall, Ca–H(BH$_3$) distances in the resultant tetramer are in the range 2.30–2.45 Å. In general, optimization leads to bond shortening with respect to the experimental structure. While all experimental B–N bond lengths in the crystal are 1.575 Å, the optimized values in the tetramer are 1.570, 1.543, and 1.527 Å in x-, y-, and z-NH$_2$BH$_3$, respectively. The respective values of Ca–N distances are 2.352, 2.400, and 2.461 Å, while in the CaAB crystal the Ca–N bond lengths are 2.383 Å.

Several initial experimental attempts of the synthesis of pure MgAB failed,[14,25] which led to the conclusion that the condensed charge on Mg^{2+} cations leads to structural instability. However, pure MgAB was finally obtained,[11] but unfortunately, the crystal structure of the compound has not been determined. A computational modelling[15] predicts that MgAB adopts a structure in the same space group as experimentally known CaAB. In the present study, we assumed the structure of $[Mg(NH_2BH_3)_2]_4$ (**1**) to be similar to that of **2**. The optimized structure of **1** (Fig. S1 in the ESI†) indeed resembles that of **2** though the pattern of the M–H(BH$_3$) contacts is slightly different. Mg–H(BH$_3$) distances are in the range 2.02–2.25 Å. Mg–N bond lengths are 2.026, 2.052 and 2.136 Å, and B–N bond lengths are 1.589, 1.592 and 1.522 Å in x-, y-, and z-NH$_2$BH$_3$, respectively.

SrAB adopts a similar structural type in the crystal as CaAB with different atomic coordinates. Positions of hydrogen atoms in the unit cell of SrAB were not determined.[13] To be consistent, we assumed the geometry of the tetrameric cluster $[Sr(NH_2BH_3)_2]_4$ (**3**) to be similar to that of **2**. In the optimized structure of **3**, Sr–H(BH$_3$) distances are in the range 2.47–2.60 Å. Sr–N bond lengths are 2.518, 2.586, and 2.632 Å, and B–N bond lengths are 1.571, 1.539, and 1.526 Å in x-, y-, and z-NH$_2$BH$_3$, respectively.

In the following discussion the energy values are reported with respect to the optimized tetrameric clusters **1**, **2**, and **3**.

B. Cleavage of B–H bonds and M_3H moiety formation

B–H dissociation energies in MAB are lower than N–H dissociation energies,[18] thus, the first obvious step in the dehydrogenation mechanism is the cleavage of the B–H bonds. Metal atoms in the considered tetramers form a diamond-shaped arrangement in the XY plane (Fig. 1b). Atomic charges of Mg from the natural population analysis are 1.398 for atoms arranged parallel to the X-axis and 1.500 $\bar{e}$ for atoms arranged parallel to the Y-axis. The respective charges of Sr are 1.157 and 1.260 $\bar{e}$. The NBO analysis provides the respective charges for Ca in **2**, 0.857 and 0.930 $\bar{e}$, to be somewhat smaller than those for Sr in **3** because of the higher natural population of valence orbitals. B–H bonds of z-NH$_2$BH$_3$ directed toward the XY plane are the longest (for example, 1.259 Å compared to 1.229 Å for other B–H bonds in this BH$_3$ group in **2**) with the largest negative charge at H atoms (NBO charges are $-0.100\ \bar{e}$; $-0.070\ \bar{e}$; and $-0.114\ \bar{e}$ for **1**, **2**, and **3**, respectively).

This journal is © the Owner Societies 2016

Phys. Chem. Chem. Phys., 2016, **18**, 31072–31077 | **31073**
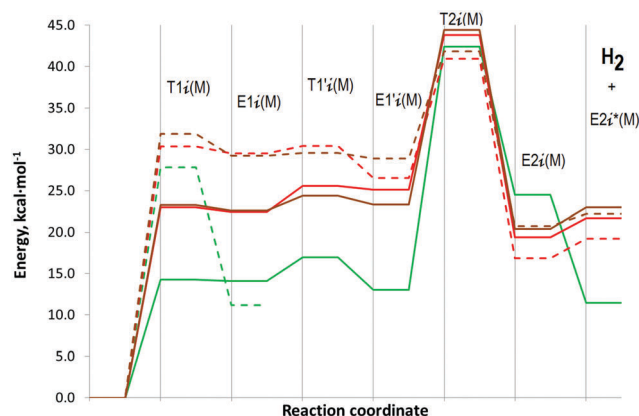
Fig. 2 Energy diagram for dehydrogenation pathways in [M(NH₂BH₃)₂]₄, M = Mg (green), Ca (red) and Sr (brown). Lines (*i* = *z*) refer to the *z*-path and dashed lines (*i* = *y*) refer to the *y*-path.

Cleavage of these B–H bonds leads to the hydrogen atom takeover by three neighboring metal cations in **E1z(M)** local minima (see the energy diagram in Fig. 2). It was shown earlier that the formation of a Li₃H moiety is a key feature of dehydrogenation pathways in LiAB.[23,24] The analogous pyramidal M₃H moiety is also formed upon activation of alkaline-earth amidoboranes. The highest bonding orbital of **E1z(Ca)** is delocalized over the Ca₃H moiety (Fig. 3). Geometrical parameters of the M₃H moieties in **E1z(M)** are provided in the ESI† (Table S1). The removed hydrogen atom gains significant charge in the environment of the three metal cations. It has a natural charge of −0.580, −0.358 and −0.484 $\bar{e}$ for M = Mg, Ca, and Sr, respectively. The transition state leading to the cleavage of the B–H bond **T1z(M)** is only slightly higher than **E1z(M)**. The energy barriers that should be crossed to split the B–H bond are 23.0 and 23.3 kcal mol⁻¹ for **2** and **3**, respectively. It is much lower for **1**, only 14.3 kcal mol⁻¹.

Alternatively, the H atom could be removed from *y*-NH₂BH₃. Transition states **T1y(M)** leading to the cleavage of the B–H bonds in such a case are higher in energy (Fig. 2, dashed lines). Activation energies are 27.8, 30.3 and 31.9 kcal mol⁻¹ for **1**, **2**, and **3**, respectively. The pathways go through the formation of a kite-shaped M₃H arrangement in **T1y(M)** and the subsequent **E1y(M)**. Similar kite-shaped Li₃H moieties were found by
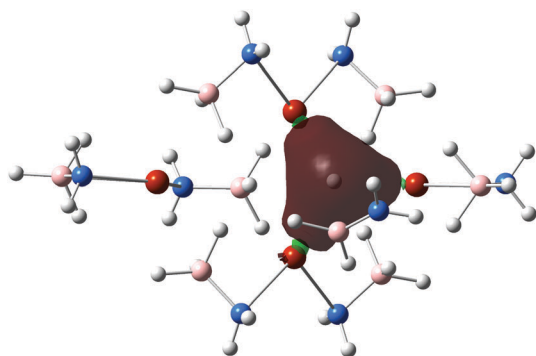
Fig. 3 The highest bonding orbital of **E1z(Ca)** local minimum. Red refers to Ca atoms, blue to N, orange to B and white to H atoms.
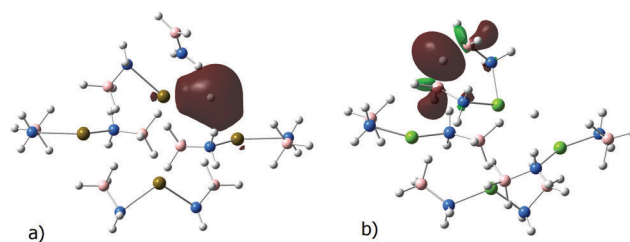
Fig. 4 Optimized structures and the highest bonding orbitals of **E1y(M)**, M = Sr (a) and Mg (b). Brown/green refers to Sr/Mg atoms, blue to N, orange to B and white to H atoms.

GRRM[26] scanning of B–H bond cleavage pathways for LiAB tetramers.[23] While intermediates **E1y(Ca)** and **E1y(Sr)** are similar, **E1y(Mg)** is quite different. The local minima **E1y(M)** are shown in Fig. 4. In the case of Ca and Sr, the highest bonding orbitals are delocalized over the removed H atom and two neighboring metal atoms, and the NH₂BH₂ intermediate is released (Fig. 4a). As in the case of the *z*-pathway, **E1y(Ca)** and **E1y(Sr)** are only slightly lower in energy than the respective transition states **T1y(M)**. In the case of Mg, the release of the NH₂BH₂ intermediate is not observed. Instead, [BH₃NH₂CaNH₂BH₂]⁺ is formed, where one H bridges two BH₂ groups (Fig. 4b). This significantly stabilizes the **E1y(Mg)** state $\left(\Delta E_0^\circ = 11.1 \text{ kcal mol}^{-1}\right)$.

C. Dehydrogenation from the same NH₂BH₃ group

Dehydrogenation implies the cleavage of N–H bonds in the NH₂BH₂ intermediate with the subsequent release of H₂ molecules. This pathway is analogous to the D-path considered by Kim *et al.*[21] for M(NH₂BH₃)₂ (M = Mg and Ca). While the first step involves the cleavage of the B–H bonds in the NH₂BH₃ group, H₂ is released in the next step *via* the M–H···H–N transition state. According to Kim *et al.*,[21] for Ca(NH₂BH₃)₂ these steps are nearly equal in energy (∼36 kcal mol⁻¹ at the MP2/6-311++G** level of theory). The dehydrogenation step for Mg(NH₂BH₃)₂ has about the same energy barrier (∼36 kcal mol⁻¹) but the cleavage of the B–H bonds proceeds more easily (∼24 kcal mol⁻¹).

The dehydrogenation steps for the *z*- and *y*-pathways are denoted as **T2z(M)** and **T2y(M)**, respectively (Fig. 2); optimized structures for M = Ca are shown in Fig. 5. IRC defines local minima, **E1′z(M)/E1′y(M)**, which are connected to **E1z(M)/E1y(M)** *via* additional steps, **T1′z(M)/T1′y(M)**, with low energy barriers between them (Fig. 2). Transition states leading to the formation of H₂ are the key states for the *z*- and *y*-pathways with activation energies ranging from 40.9 to 44.4 kcal mol⁻¹ (Fig. 2). The M₃H pyramidal moiety in **T2z(M)** and the M₃H kite-shaped arrangement in **T2y(M)** are destroyed (Fig. 5a). The hydrogen atoms in the transition states are located between two M atoms. The destruction of the M₃H pyramidal moiety requires somewhat higher energy barriers. The **T2z(M)** energies increase in the order Mg < Ca < Sr. It should be noted that the IRC scan leads to the intermediate **E2z(Mg)**, which is somewhat different from **E2z(Ca)** and **E2z(Sr)** (see the ESI,† Fig. S2).

While **E2z(Ca)** and **E2z(Sr)** are lower in energy with respect to **E2z*(M)** and free H₂ molecules, **E2z(Mg)** is higher in energy (Fig. 2).

31074 | *Phys. Chem. Chem. Phys.*, 2016, **18**, 31072–31077

This journal is © the Owner Societies 2016
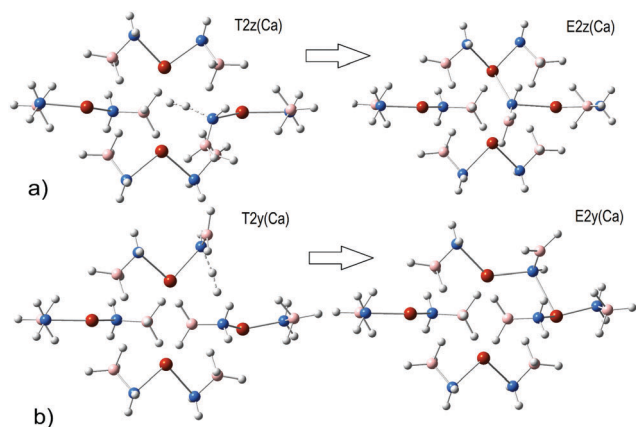
Fig. 5 Transition states and the final products for z- (a) and y- (b) pathways for $[Ca(NH_2BH_3)_2]_4$.

Fig. 6 Oligomerization z-pathway for $[Ca(NH_2BH_3)_2]_4$. Dashed lines show the Ca_3H pyramidal moiety. For **E3z(Ca)**, the number of sites of NH_2 groups is shown.

For the sake of comparison, we also explored a direct dehydrogenation pathway which proceeds through hydrogen evolution *via* $N-H^{\delta+}\cdots H^{\delta-}-B$ interaction in the same NH_2BH_3 group. This pathway was found to be the most favorable for the CaAB dimer in the theoretical study of Yuan *et al.*[22] (TS could be as low as 21.7 kcal mol^{-1} computed within an extended unit cell PBE/PAW method). The direct intramolecular dehydrogenation pathway was also assumed for CaAB and MgAB thermal decomposition in the theoretical study of Wang *et al.*[16] The release of the first H_2 molecule requires to overcome a barrier of 69.0 kcal mol^{-1} for MgAB and 73.5 kcal mol^{-1} for CaAB at the CCSD(T)/6-311++G(3d,2p) level of theory.[16] In the present study on the example of **2** we found this pathway to be the most energetically demanding. The energy of the $N-H\cdots H-B$ transition state (Fig. S3 in the ESI†) leading to the release of the first H_2 molecule from x-NH_2BH_3 is 59.7 kcal mol^{-1}. Optimization of the corresponding transition states for y- and z-NH_2BH_3 converged to the alternative transition states **T2z(M)**/**T2y(M)** considered above.

D. Oligomerization pathways

An oligomerization pathway going through $B-N$ bond formation between NH_2BH_3 and NH_2BH_2 units was found to be the most favorable in the case of LiAB tetramers.[23] Compared with the D-path, the O-path was found to be more favorable for LiAB, KAB, and NaAB dimers and less favorable for CaAB and MgAB monomers in Kim's study.[21]

For tetramers, considered in the present work, $B-N$ bond formation between NH_2BH_3 and NH_2BH_2 units can proceed along both z- and y- pathways. Oligomerization pathways are structurally similar for M = Mg, Ca and Sr. As an example, structural transformation leading to the $B-N$ bond formation along the z-pathway is shown in Fig. 6 for M = Ca. The Ca_3H moiety is retained along the oligomerization pathway. Structural transformations along the y-pathway are analogous (ESI,† Fig. S4). The energy diagram is presented in Fig. 7. **T3y(M)** energies in the oligomerization step (30.5 and 33.2 kcal mol^{-1} for M = Ca and Sr, respectively) are similar to those leading to the cleavage of the $B-H$ bonds. For the z-pathway the oligomerization step is more energetically demanding than the first **T1z(M)** step by
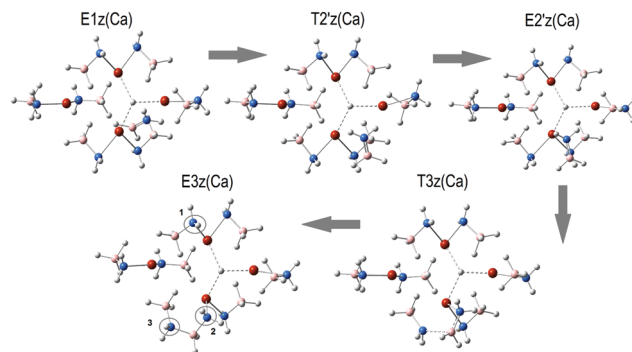
3–5 kcal mol^{-1}, but somewhat lower in energy than the oligomerization step for the y-pathway. Energies of **T3z(M)** are 17.3, 26.4, and 28.0 kcal mol^{-1} for M = Mg, Ca and Sr, respectively. Formation of the $B-N$ bond significantly stabilizes **E3z(M)** though it is still notably endothermic for M = Ca and Sr. In contrast, formation of **E3z(Mg)** is slightly exothermic (-0.2 kcal mol^{-1}), and after an isomerization step *via* **T3′z(Mg)**, formation of the **E3′z(Mg)** product is exothermic by -8.1 kcal mol^{-1} (see Fig. 7).

The dehydrogenation step implies further cleavage of $N-H$ bonds. Possible sites of involved NH_2 groups are shown in Fig. 6 for the product **E3z(M)**. Five transition states found for the dehydrogenation of **E3z(Ca)** are given in Fig. S5, ESI.† Energies of **T4z(Ca)** vary from 43 to 53 kcal mol^{-1}. The dehydrogenation transition states **T4z(M)** in the oligomerization pathway are higher in energy than **T2z(M)** in the pathway avoiding the oligomerization step, similar to previous findings for the alkaline-earth amidoborane monomers.[21]

The lowest energy barrier corresponds to the transition state leading to the hydrogen release from site number 3 where the NH_2 group is associated with two B atoms. The transition state,
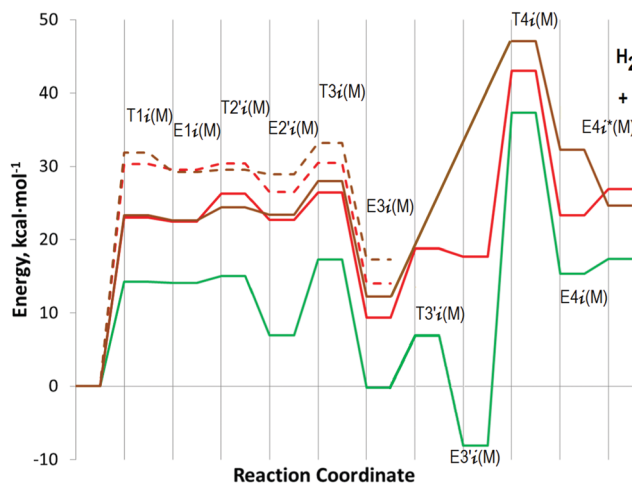
Fig. 7 Energy diagram of oligomerization pathways for $[M(NH_2BH_3)_2]_4$, M = Mg (green), Ca (red) and Sr (brown). Lines (i = z) refer to the z-path and dashed lines (i = y) refer to the y-path.

This journal is © the Owner Societies 2016

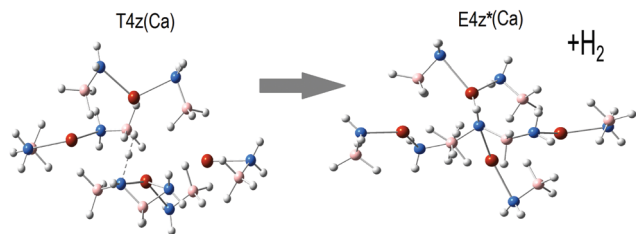*Phys. Chem. Chem. Phys.*, 2016, **18**, 31072–31077 | 31075

Fig. 8 The lowest transition state, **T4z(Ca)**, and the product of H$_2$ release, **E4z*(Ca)**, from [Ca(NH$_2$BH$_3$)$_2$]$_4$ via an oligomerization pathway.

T4z(Ca), and its product **E4z*(Ca)** are shown in Fig. 8. Similar transition states also exist in the case of Mg and Sr. The energies of the states are 37.3, 43.0 and 47.1 kcal mol^{-1} for M = Mg, Ca and Sr, respectively. The final product of the step is notably endothermic for all considered tetramers; $\Delta E_0^{\circ}(\textbf{E4z*}(\textbf{M})+\textbf{H}_2)$ is 17.4, 26.9, and 24.6 for M = Mg, Ca, and Sr, respectively.

It should be noted that the energy of the lowest dehydrogenation transition state from the [LiNH$_2$BH$_3$]$_4$ cluster is 31.2 kcal mol^{-1} at the M06/6-311(d,p) computational level. The energy of the lowest transition state leading to the oligomerization is 25.5 kcal mol^{-1}.[23] Analogous values for tetramer **2** at the same level of theory are 42.6 **T4z(Ca)** and 26.0 **T3z(Ca)** kcal mol^{-1}. While oligomerization in the case of [Ca(NH$_2$BH$_3$)$_2$]$_4$ needs to overcome nearly the same energy barrier as that in the case of [LiNH$_2$BH$_3$]$_4$, the dehydrogenation step is significantly more energy consuming. Presumably the reason is the better mobility of the closed shell LiH unit formed after the cleavage of the B–H bond. In contrast to LiAB tetramers, the diamond-shaped arrangement of metal atoms in **2** is maintained in the cluster during all transformations in the reaction direction.

While H$_2$ elimination is a major result of thermal decomposition of MAB, some amount of ammonia release is observed experimentally.[6,7,13] According to the mechanisms of the thermal decomposition of the alkali-metal amidoboranes suggested by Fijalkowski *et al.*,[8] this secondary NH$_3$ release proceeds via the B–N bond cleavage accompanied by intermolecular transfer of H$^{\delta+}$ and intermediate formation of weakly bonded [MNH$_3$]$^+$ cations. To estimate whether the cleavage of B–N bonds in alkaline-earth metal amidoboranes is a competitive process with the H$_2$ elimination mechanisms suggested above, we considered several B–N bond breaking pathways in **2**. Three different transition states leading to the cleavage of B–N bonds of z-NH$_2$BH$_3$ are provided in the ESI† (Fig. S6). One of the possibilities, **T5z(Ca)**, leads to the formation of [CaNH$_3$]$^+$ cations in **E5z(Ca)**. However, the activation energy is 81.1 kcal mol^{-1}, *i.e.* 3.5 times larger than the activation energy of B–H bond cleavage via **T1z(Ca)**, and about twice as large as that of the key state for H$_2$ release via the oligomerization pathway, **T4z(Ca)**. Transfer of BH$_3$ to one of the y-NH$_2$BH$_3$ units is accompanied by the occupation of the [NH$_2$]$^-$ residue at the position between three Ca atoms forming a pyramidal Ca$_3$NH$_2$ moiety analogously to the Ca$_3$H moiety discussed above. One of the transition states, **T6z(Ca)** with an energy of 50.8 kcal mol^{-1}, leads to bridging of the released BH$_3$ with the BH$_3$ group of y-NH$_2$BH$_3$ by the H atom. The other transition state, **T7z(Ca)** with an energy of

51.3 kcal mol^{-1}, leads to head-to-tale dimerization with the formation of a [BH$_3$NH$_2$BH$_3$]$^-$ unit. Thus, it follows that B–N bond breaking pathways have larger activation energies than H$_2$ elimination pathways. This is consistent with the minor role of mechanisms leading to the release of ammonia.

Computational details

The conventional transition state theory was used to predict the optimized structures and transition states of [M(NH$_2$BH$_3$)$_2$]$_4$ tetramers, where M = Mg, Ca, and Sr. The intrinsic reaction coordinate (IRC) scans confirmed the connectivity of all the transition states to reactants and products of a given step. It was noted in previous theoretical investigations that taking into account van der Waals interactions is important to reproduce experimental parameters of SrAB.[20] All computations were performed within DFT using the M06[27] functional, which takes dispersion interaction into account. The TZVP[28] basis set was used throughout. The same computation level was used for the Natural Bond Orbital (NBO) analysis.[29] The Gaussian 09 code[30] was utilized in all computations.

Conclusion

A cluster approximation was used to explore the release of the first H$_2$ molecule from alkaline-earth metal amidoboranes. To form the cluster, geometries of four neighboring molecules were extracted from a layer of experimental crystal structure of CaAB. The cleavage of B–H bonds in the NH$_2$BH$_3$ unit in the environment of alkaline-earth metal atoms leads to the "capture" of the released H atom by neighboring metal atoms with the formation of a M$_3$H moiety. Such a moiety was found to be a key feature of the dehydrogenation process in small (trimeric and tetrameric) LiAB clusters.[23,24] The formation of this Li$_3$H moiety was ascribed to the existence of stable Li$_3$H clusters.[31,32] Despite the fact that similar free M$_3$H clusters are not found in alkaline-earth metal hydrides (unlike Li$_3$H, Ca$_3$H is an open shell construct), the M$_3$H moiety (M = Mg, Ca, and Sr) plays an important role in the structural transformations of alkaline-earth metal amidoboranes. The M$_3$H moiety has a delocalized bonding orbital and the M–H bond lengths are only slightly larger than the sum of the respective covalent radii.

While the cleavage of the B–H bonds and further oligomerization of amidoboranes require moderate energy, the cleavage of N–H bonds accompanied by destruction of the M$_3$H moiety in favor of H$_2$ formation is much more energy consuming. This step requires significant energy uptake both for oligomerization and non-oligomerization pathways.

Kinetically, after the cleavage of the first B–H bond, the cleavage of other B–H bonds or/and oligomerization with B–N bond formation require much less energy uptake than a direct H$_2$ release. This indicates that compounds featuring MNH$_2$BH$_2$NH$_2$BH$_3$ units are potential intermediates in the dehydrogenation process. The large number of possible isomers of such compounds makes the use of a convenient transition state method ineffective for

31076 | *Phys. Chem. Chem. Phys.*, 2016, **18**, 31072–31077

This journal is © the Owner Societies 2016

the exploration of pathways for the release of second and subsequent hydrogen molecules. In such a situation, use of the GRRM[26] method is recommended for further studies.

The cleavage of B–N bonds is found to be significantly less favorable than the cleavage of B–H bonds. If local overheating leads to the B–N bond cleavage, then the formation of the M_3NH_2 moiety is more favorable than the formation of the MNH_3 complex. This may be accompanied by the formation of an intermediate $[BH_3NH_2BH_3]^-$ or the release of diborane. The following NH_3 release is likely to be a multistep side process which requires additional studies which are outside the scope of the present research.

Tetramers of alkaline-earth metal (Mg, Ca and Sr) amidoboranes show similar tendencies along the reaction pathways with energy barriers increasing in the order Mg < Ca ≤ Sr. However, according to experiments,[11] a higher temperature is required for the start of the dehydrogenation in the case of MgAB, which suggests a larger barrier for H_2 release from MgAB compared to CaAB and SrAB. One of the reasons for this disagreement could be our assumption of a similar crystal structure for MaAB and CaAB, and, consequently, a similar local environment of the atoms in tetramer clusters **1** and **2**. Note that previous computational studies based on such an assumption also resulted in lower energy barriers for the thermal decomposition of MgAB compared to CaAB.[18] In the present study, we demonstrate that unlike Ca and Sr, in the case of Mg, oligomerization of NH_2BH_3 and NH_2BH_2 units in **1** makes the formation of the **E3′z (Mg)** intermediate exothermic and significantly increases the activation energy for the subsequent dehydrogenation steps. We suppose that similar transformations occur in the crystal structure of MgAB prior to the dehydrogenation which increases the overall activation energy for MgAB dehydrogenation compared to CaAB and SrAB.

Acknowledgements

References

1 W. Grochala and P. P. Edwards, *Chem. Rev.*, 2004, **104**, 1283.

2 S. Orimo, Y. Nakamori, J. R. Eliseo, A. Züttel and C. M. Jensen, *Chem. Rev.*, 2007, **107**, 4111.

3 Y. S. Chua, P. Chen, G. Wua and Z. Xionga, *Chem. Commun.*, 2011, **47**, 5116.

4 R. Owarzany, P. J. Leszczyński, K. J. Fijalkowski and W. Grochala, *Crystals*, 2016, **6**, 88.

5 Z. Xiong, C. K. Yong, G. Wu, P. Chen, W. Shaw, A. Karkamkar, T. Autrey, M. O. Jones, S. R. Johnson, P. P. Edwards and W. I. F. David, *Nat. Mater.*, 2008, **7**, 138.

6 K. J. Fijalkowski and W. Grochala, *J. Mater. Chem.*, 2009, **19**, 2043.

7 K. J. Fijalkowski, R. V. Genova, Y. Filinchuk, A. Budzianowski, M. Derzsi, T. Jaroń, P. J. Leszczyński and W. Grochala, *Dalton Trans.*, 2011, **40**, 4407.

8 K. J. Fijalkowski, T. Jaroń, P. J. Leszczyński, E. Magos-Palasyuk, T. Palasyuk, M. K. Cyrańskic and W. Grochala, *Phys. Chem. Chem. Phys.*, 2012, **14**, 5778.

9 K. J. Fijalkowski, R. Jurczakowski, W. Koźmińskia and W. Grochala, *Phys. Chem. Chem. Phys.*, 2014, **16**, 23340.

10 R. Owarzany, K. J. Fijalkowski, T. Jaroń, P. J. Leszczyński, Ł. Dobrzycki, M. K. Cyrański and W. Grochala, *Inorg. Chem.*, 2016, **55**, 37.

11 J. Luo, X. Kang and P. Wang, *Energy Environ. Sci.*, 2013, **6**, 1018.

12 H. Wu, W. Zhou and T. Yildirim, *J. Am. Chem. Soc.*, 2008, **130**, 14834.

13 Q. G. Zhang, C. X. Tang, C. H. Fang, F. Fang, D. Sun, L. Z. Ouyang and M. Zhu, *J. Phys. Chem. C*, 2010, **114**, 1709.

14 H. V. K. Diyabalanage, R. P. Shrestha, T. A. Semelsberger, B. L. Scott, M. E. Bowden, B. L. Davis and A. K. Burrell, *Angew. Chem., Int. Ed.*, 2007, **46**, 8995.

15 Y. Zhang and C. Wolverton, *J. Phys. Chem. C*, 2012, **116**, 14224.

16 K. Wang, V. Arcisauskaite, J.-S. Jiao, J.-G. Zhang, T.-L. Zhang and Z.-N. Zhou, *RSC Adv.*, 2014, **4**, 14624.

17 Y. Zhang, T. Autrey and C. Wolverton, *J. Phys. Chem. C*, 2012, **116**, 26728.

18 W. Li, G. Wu, Y. Chua, Y. P. Feng and P. Chen, *Inorg. Chem.*, 2012, **51**, 76.

19 C. B. Lingam, K. R. Babu, S. P. Tewari, G. Vaitheeswaran and S. Lebègue, *J. Phys. Chem. C*, 2011, **115**, 18795.

20 B. L. Chittari and S. P. Tewari, *Mater. Chem. Phys.*, 2014, **148**, 364.

21 D. Y. Kim, H. M. Lee, J. Seo, S. K. Shin and K. S. Kim, *Phys. Chem. Chem. Phys.*, 2010, **12**, 5446.

22 P.-F. Yuan, F. Wang, Q. Sun, Y. Jia and Z. X. Guo, *Int. J. Hydrogen Energy*, 2013, **38**, 11313.

23 A. V. Pomogaeva, K. Morokuma and A. Y. Timoshkin, *J. Phys. Chem. A*, 2016, **120**, 145.

24 A. V. Pomogaeva, K. Morokuma and A. Y. Timoshkin, *J. Comput. Chem.*, 2016, **37**, 1259.

25 Y. S. Chua, G. Wu, Z. Xiong, A. Karkamkar, J. Guo, M. Jian, M. W. Wong, T. Autrey and P. Chen, *Chem. Commun.*, 2010, **46**, 5752.

26 S. Maeda, K. Ohno and K. Morokuma, *Phys. Chem. Chem. Phys.*, 2013, **15**, 3683.

27 Y. Zhao and D. G. Truhlar, *Theor. Chem. Acc.*, 2008, **120**, 215.

28 F. Weigend and R. Ahlrichs, *Phys. Chem. Chem. Phys.*, 2005, **7**, 3297.

29 E. D. Glendening, A. E. Reed, J. E. Carpenter and F. Weinhold, NBO Version 3.1.

30 M. J. Frisch, G. W. Trucks, H. B. Schlegel, G. E. Scuseria, M. A. Robb, J. R. Cheeseman, G. Scalmani, V. Barone, B. Mennucci and G. A. Petersson, *et al.*, *Gaussian 09, Revision C.01*, Wallingford, CT, 2009.

31 C. H. Wu and R. O. Jones, *J. Chem. Phys.*, 2004, **120**, 5128.

32 J. A. Jr. Montgomery, H. H. Michels, O. F. Guner and K. Lammertsma, *Chem. Phys. Lett.*, 1989, **161**, 291.

This journal is © the Owner Societies 2016

Phys. Chem. Chem. Phys., 2016, **18**, 31072–31077 | 31077